11. A. G. Eguiluz, A. A. Maradudun, R. J. Elliott, *Phys. Rev. B* **27**, 4933 (1983); S. T. Chui and B. Tanatar, *Phys. Rev. Lett.* **74**, 458 (1995).
12. S. V. Kravchenko, D. Simonian, M. P. Sarachik, W. Mason, J. E. Furneaux, *ibid.* **77**, 4938 (1996); Y. Hanein *et al.*, *ibid.* **80**, 1288 (1998).
13. J. P. Eisenstein, L. N. Pfeiffer, K. W. West, *ibid.* **68**, 674 (1992).
14. L. S. Levitov, personal communication; see also V. M. Bedanov and F. M. Peeters, *Phys. Rev. B* 49, 2667 (1994); R. Egger, W. Hausler, C. H. Mak, H. Grabert, cond-mat/9903111.
15. Y. Wan, G. Ortiz, P. Phillips, *Phys. Rev. Lett.* **75** 2879 (1995); M. E. Raikh and L. I. Glazman, *ibid.* **77**, 1354 (1996); A. A. Koulakov and B. I. Shklovskii *Phys. Rev. B* **57**, 2352 (1998); D. L. Miller, cond-mat/9808103.
16. Supported by the Office of Naval Research, the Packard Foundation, the National Science Foundation DMR, the Massachusetts Institute of Technology Center for Materials Science and Engineering, and JSEP. We thank L. S. Levitov, M. A. Kastner, and P. A. Lee for illuminating discussions.

5 March 1999; accepted 22 June 1999

Fault Slip Rates at Depth from Recurrence Intervals of Repeating Microearthquakes

Robert M. Nadeau and Thomas V. McEvilly

Unique attributes in sequences of recurring, similar microearthquakes at Parkfield, California, provide a means for inferring slip rate at depth throughout the active fault surface from the time intervals between sequence events. Application of the method using an 11-year microseismicity record revealed systematic spatial and temporal changes in the slip rate that were synchronous with earthquake activity and other independent measures of fault-zone slip. If this phenomenon is found to be generally common behavior in active faults, it forms the basis for a method to monitor the changing strain field throughout a seismogenic fault zone.

Microearthquake data since 1987 at Parkfield, California, include more than 6000 small events (moment magnitudes in the range of -1 to 5) along a heavily instrumented segment of the San Andreas fault (*1*). An organized mode of seismic fault slip was detected by the borehole seismographic network there (*2*). Most ongoing seismicity can be organized in space and time into about 300 small clusters of microearthquake activity within the fault zone. Most clusters contain sequences of as many as 20 similar, regularly occurring, ("characteristic") microearthquakes (Fig. 1) identified by waveform cross-correlation coefficients >0.98 between pairs of events. The sequences appear to represent repeating slip on adjacent but nonoverlapping patches <20 m wide. More than 99% of the fault surface appears to be slipping without detectable earthquakes. Time intervals between characteristic microearthquakes range from a few months to a few years and scale with event size.

The measured seismic moment–release rate in repeating sequences has been combined with the geodetically determined tectonic loading rate to estimate earthquake source parameters that follow simple scaling relations and describe a fault that is locally strong (kilobar-range stress drops at dimensions of <100 m) but weak at the 10- to 20-km crustal scale of larger earthquakes (*3*). In this model the clusters define local strength concentrations, or asperities, within the fault zone. We view the recurrence rates in repeating sequences as indicators of the rate of fault slip at depth (*4*).

Earth Sciences Division, Lawrence Berkeley National Laboratory, and Berkeley Seismological Laboratory, University of California, Berkeley, CA 94720, USA.

A period of increased earthquake activity began in October 1992 and included the four largest events that occurred since 1987 (magnitudes 4.2, 4.6, 4.7, and 5.0). These earthquakes with their aftershock sequences produced a transient slip on a 25 km^2 strip that includes the hypocenter of the most recent magnitude 6 earthquake at Parkfield. Summing moments over the total area, the relation $M = GAs$ among scalar seismic moment (M), shear modulus at the fault (G), slip area (A), and fault slip (s) yields an average slip over the strip of 10 to 20 cm for the sequence, consistent with values obtained by deconvolution of locally recorded accelerograms (*5*). Other deformation-related changes were reported during this period of activity (*6, 7*).

Changes in previously stable recurrence rates for many repeating sequences began in 1992. This apparent connection between the localized slip in the large earthquakes and the recurrence rates throughout the fault zone motivated our study of recurrence changes and fault slip rate. We identified 160 repeating sequences containing three or more events for a total of 1004 individual microearthquakes, and 844 recurrence interval times. To characterize variability, we computed M from the observed waveforms for each earthquake and measured the recurrence interval, T, for every pair of time-adjacent events in a sequence. These two parameters were averaged for each of the sequences to normalize the M and T values (Fig.

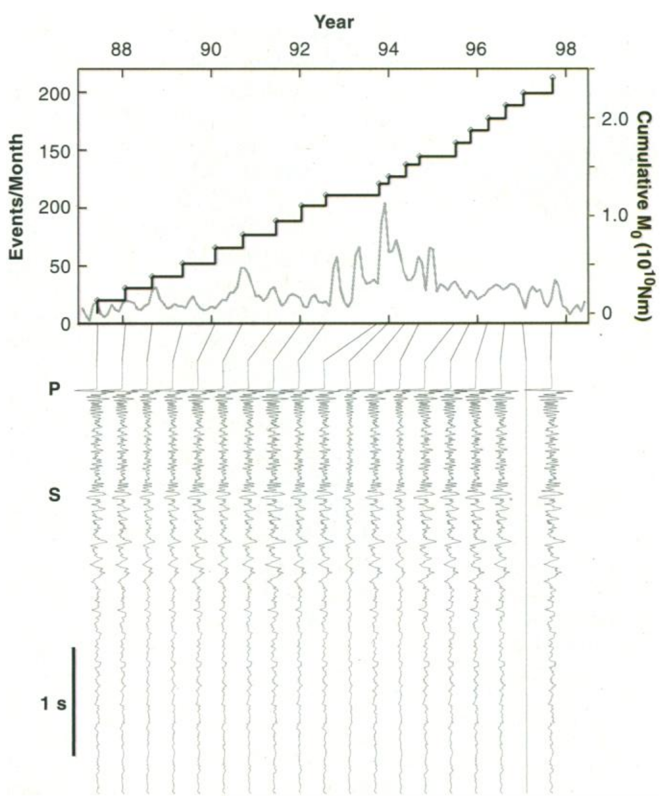

Fig. 1. The upper panel shows the cumulative seismic moment for a sequence of similar microearthquakes (right) and the rate of total seismicity for Parkfield. The lower panel shows example vertical component seismograms for the sequence from borehole station VCA (inoperative for event 18).

2). The similarity in source size for microearthquakes in a sequence is evident in the narrow distribution of M/M_{av} ("av" indicates average value). The distribution for T/T_{av} for the full data set is broadened by two phenomena that have little effect on the distribution of M: missing sequence members and the abrupt shift in 1992 in recurrence times. The former puts erroneous long intervals in the distribution, and the latter suggests a changing slip rate. Both factors would distort an otherwise sharp T/T_{av} distribution toward the shape actually observed (*8*).

The unvarying source function among sequence members is evidence for a process in which the tectonic loading rate on the fault drives the variation in recurrence time of repeating, similar microearthquakes in a near steady-state process. Similarity of repeating waveforms to the highest frequencies observed (125 Hz) implies that A is constant for events in a sequence, and we used the values of A derived from the geodetic loading rate (*3*) to calculate absolute slip rates from relative estimates. We assumed that G remains constant for rocks within the San Andreas fault zone in the vicinity of any recurring sequence. In this model, changes in the rate of moment release, $\dot{M}$, and the corresponding rate of fault slip, $\dot{s}$, are revealed in the variations of recurrence interval within a repeating sequence of events. Within a given sequence and during a specific recurrence interval, T_i, we determine the average slip rate at the sequence site

$$\dot{s}_{av} = \dot{M}/GA = M_{av}/GAT_i \qquad (1)$$

using the average moment for the sequence (*9*).

Variations in T/T_{av} correlate for nearby sequences. We took advantage of this local coherence to smooth the estimates of recurrence time variations by processing the data in ensembles of nearby sequences. We determined ensemble-averaged slip rates at 6-month intervals with spatial sampling on a circle of radius 2 km moved horizontally and vertically throughout the fault plane in 250-m steps, thus constructing a spatial-temporal distribution of slip rates. We compared the spatial distribution of average annual slip rate along the fault zone above 5 km to the fault-parallel deformation measured geodetically on Earth's surface (*10*), and to the direct measurements of fault slip by creepmeters installed across the fault trace on the surface (*11*). The recurrence-derived slip rate profile for the shallow fault zone is consistent with these surface observations, showing the transition from creeping to locked behavior southeastward along the fault (Fig. 3).

Changes in computed slip rates were greatest in sequences near the large 1992 to 1994 earthquakes, but they occurred at distances more than 10 km from that region and throughout the full vertical extent (3 to 12 km depths) of seismic activity. The maximum gradient in average slip rate was found in the vertical direction at the 1966 hypocenter, where the rate increased from 1.5 to 3.5 cm/year between 7 and 10 km depth (Fig. 3). We calculated changes in the spatial patterns of derived slip rates, using the October 1989 pattern as a reference (Fig. 4). From April 1988 to October 1990, a slip-rate increase of about 1.0 cm/year occurred at the northwest edge of the study area. A perturbation in slip rate greater than 1.5 cm/year commenced late in 1990 (with the 10/90 frame in Fig. 4) in the deep region (>6 km) around the 1966 hypocenter. As slip rates increased in the vicinity of the impending large earthquakes, slip rate was decreasing by about 1 cm/year in the

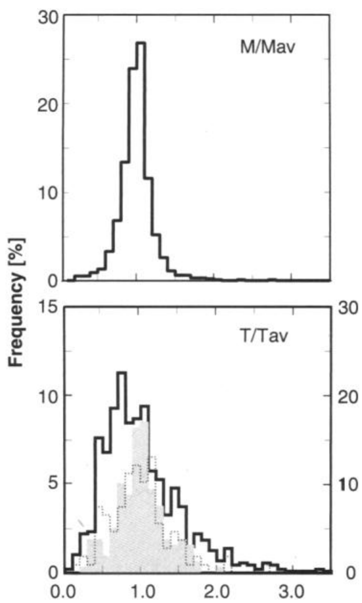

Fig. 2. Distributions of sequence-normalized seismic moments (top) and recurrence intervals (bottom) for 160 sequences. Coefficients of variation (COVs) for moments and intervals are 0.22 and 0.49, respectively, for the full data set (black lines). COVs for recurrence intervals are 0.42 and 0.32, respectively, for subsets (right scale) of larger (magnitude > 1.0) events (broken line) and events before June 1992 (shaded area).

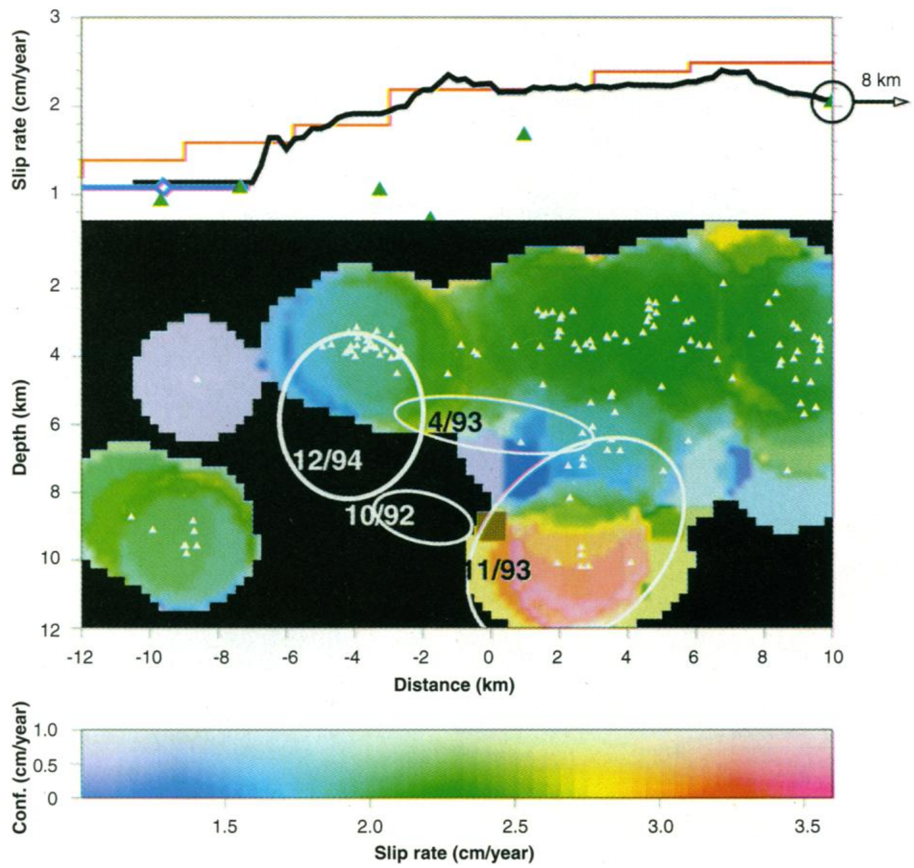

Fig. 3. The N45°W fault zone section showing average annual slip rate from recurrence intervals compared with surface measurements (distance in kilometers NW). White triangles, sequence locations; white ellipses, locations of large 1992–1994 earthquakes and their aftershocks, with dates centered on the mainshock locations; brown square, 1966 magnitude 6 hypocenter at 35.955°N, 120.498°W; black curve, profile of median recurrence-derived slip rate taken above 5 km depth; red curve, geodetically measured rate (*10*); green triangles, surface slip rates from creepmeters (*11*); open blue diamond and bar, two-color geodimeter measurement and array location, respectively (*13*). Color intensity of the slip-rate scale is keyed to the confidence limits in the slip-rate estimates.

northwest zone, reversing the earlier 1988 to 1990 increase in that region. In 1995, slip rates returned to their pre-1991 levels in both regions, and a zone of increased slip rate had progressed from the deep region upward and to the southeast in the fault zone. The pulse of increased slip appears to have moved through the southeastern edge of the study area by the 10/97 frame, after which the data are too sparse to define the slip rate throughout the complete fault zone (*12*). The diminished remaining coverage in 1998 is still adequate to show that the shallow zone (<6 km) of very high slip rate in 1994 had returned to the 1989 rate or less by 1998.

The fraction of repeating microearthquakes in the deep seismicity (the box in frame 10/97 in Fig. 4) varied in a cyclic manner throughout the monitoring period, reaching a peak value of 68% in 1989 and decreasing thereafter. In 1988 this fraction varied in phase with total activity in the region, but subsequently the relation shifted to one in which steep declines in the fraction of repeating events occurred at times of increasing total seismicity in 1990, 1992, and 1993. After its 1989 maximum, throughout the 1992 to 1994 activity, the fraction fell with each distinct increase in total earthquake occurrence, subsequently rising again, but to successively lower peak values. After 1994, the repeating and nonrepeating seismicity declined together and the fraction of repeating events varied in the 0 to 10% range, the lowest levels in the study period. Repeating events and inferred fault slip ceased completely in the region in 1997.

Recurrence-derived slip-rate changes were compared with deformation along the fault zone obtained by two-color geodimeter baseline measurements taken several times weekly since mid-1984 (*7, 13*). The two independent estimates are qualitatively consistent in Fig. 5, considering that the geodimeter data were acquired near the locked section of the fault and are contaminated by yearly oscillations due to seasonal wetting and drying of the soil at the monuments (*13*).

Estimating fault slip at depth from surface observations alone is a poorly resolved, in-

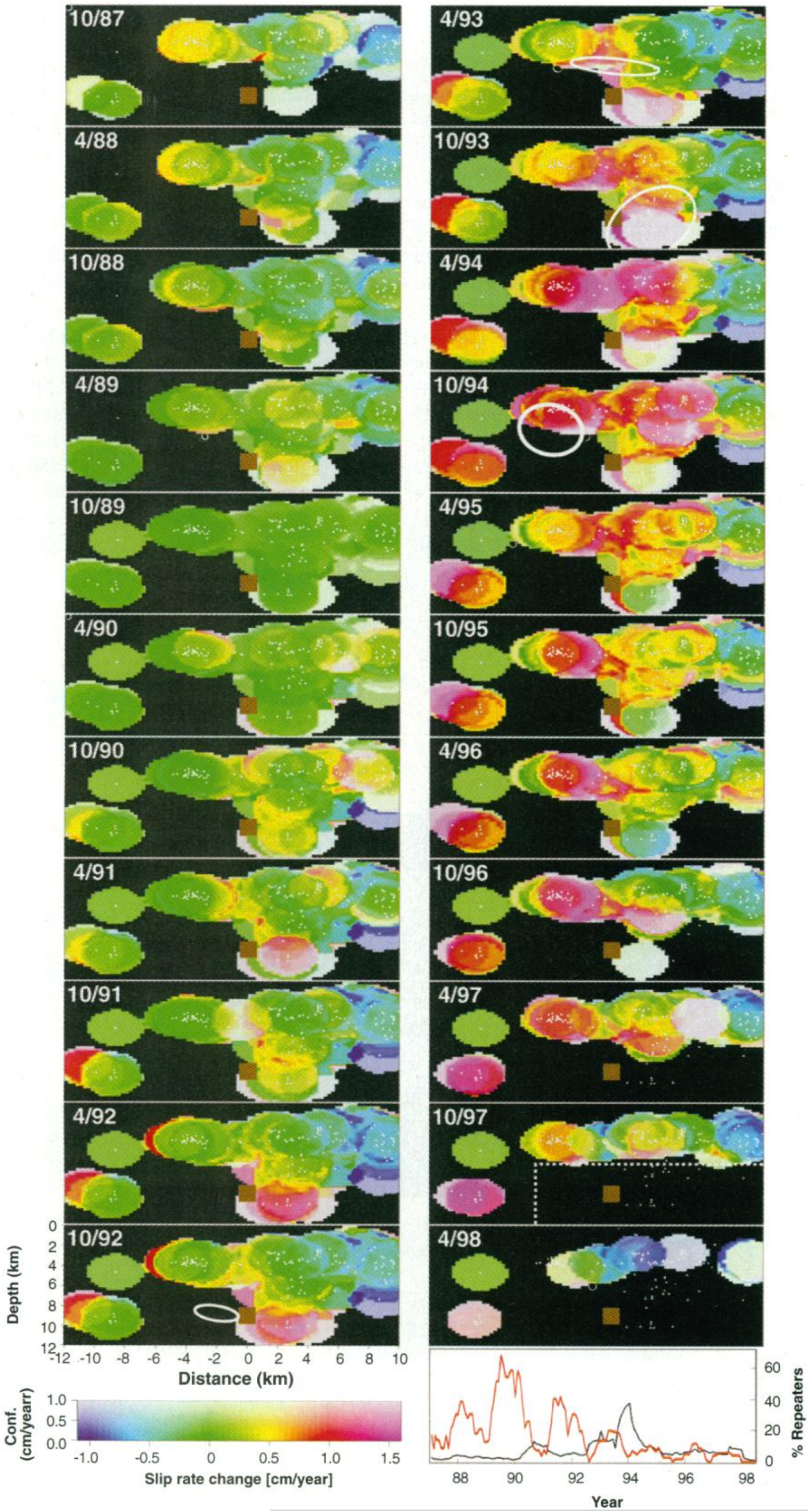

Fig. 4. Slip-rate change in 6-month snapshots. Symbols are as for Fig. 3 and distance is in kilometers to the northwest. Color scale hue shows change in slip rate relative to 10/89, and intensity represents confidence limits. The curves in the lowermost frame track the fraction of repeating events (red) and total seismicity (black) for the deep box in the 10/97 frame.

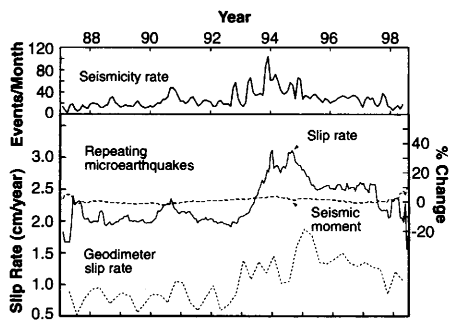

Fig. 5. (Top) Seismicity rate smoothed with a 2-month running window. (Center) Variations in recurrence-derived slip rate (solid) and sequence-normalized seismic moment (dashed) for the 160 sequences studied. The left scale is absolute slip rate, and the right scale is relative change in slip rate and moment. (Bottom) Slip rate from the two-color laser geodimeter (*7, 13*) at the location shown in Fig. 3.

verse problem (*7, 10, 13, 14*). Slip rates at depths of the repeating sequences cannot be resolved by other methods, so recurrence-determined rates in joint inversion with surface deformation can provide constraints for fault slip throughout the full depth range of the fault. With microearthquake observations made at distances of 10 to 20 km slip-rate, changes of a few millimeters per year can be resolved. We view each sequence as a point detector of local slip on the fault.

Our analysis suggests that a propagating concentration of accelerated slip entered the Parkfield segment of the San Andreas fault from the northwest in 1988 and moved along the fault zone to the southeast, leaving the area in 1998. It moved through the hypocentral region of the most recent magnitude 6 Parkfield earthquakes, triggering a succession of increasingly energetic episodes of slip-induced seismicity, and culminated with near complete relaxation in that region. The only part of the fault showing slip rates in 1998 greater than pre-1989 levels was the southeasternmost section at 8 to 10 km depth, as if the slip pulse had moved beneath the locked section of the fault. Throughout all this change, the repeating microearthquake waveforms did not vary measurably, precluding substantial change in earthquake source parameters or medium properties at the sources. Local conditions, other than loading rates, remained essentially constant at the asperities, and processes that would result in fluctuations in source size, such as fault strengthening with contact time (fault healing), although detectable, were very small (*15*).

The utility of the recurrence-derived slip-rate distribution lies in its monitoring potential for processes at depth in active fault zones. It remains to be determined whether the correlation of slip-rate variations and microearthquake occurrence found at Parkfield exists elsewhere, if the method can be extended in time (to decades and centuries) and space (hundreds of kilometers) for application to large damaging earthquakes, and whether the precursory changes in the relative abundance of repeating sequences of microearthquakes is a basic phenomenon in the earthquake cycle. There are few high-resolution networks in place today to test this at magnitudes approaching zero, where recurrence times are less than a few years and thus readily detected.

References and Notes

1. W. H. Bakun and A. G. Lindh, *Science* **229**, 619 (1985).
2. R. M. Nadeau, W. Foxall, T. V. McEvilly, *ibid.* **267**, 503 (1995); R. M. Nadeau and T. V. McEvilly, *Bull. Seismol. Soc. Am.* **87**, 1463 (1997).
3. R. M. Nadeau and L. R. Johnson, *Bull. Seismol. Soc. Am.* **88**, 790 (1998).
4. W. L. Ellsworth, in *Urban Disaster Mitigation: The Role of Science and Technology*, F. Y. Cheng and M. S. Sheu, Eds. (Elsevier, Oxford, 1995); D. P. Schaff, G. C. Beroza, B. E. Shaw, *Geophys. Res. Lett.* **25**, 4549 (1998). In sequences of similar aftershocks, seismic moment release and recurrence rates were related to measured surface deformation and loading rate at depth to investigate post-seismic deformation. An aftershock sequence differs from the more nearly steady-state microearthquake occurrence seen at Parkfield.
5. J. B. Fletcher and P. Spudich, *J. Geophys. Res.* **103**, 835 (1998).
6. E. Karageorgi, T. V. McEvilly, R. Clymer, *Bull. Seismol. Soc. Am.* **87**, 39 (1997); E. G. Quilty and E. A. Roeloffs, *ibid.*, p. 310.
7. J. Langbein, R. Gwyther, R. Hart, M. T. Gladwin, *Geophys. Res. Lett.*, in press.
8. The triggered network can fail to capture an event for a number of reasons, introducing artificially lengthened T_{av} and (typically doubled) T values. The bimodal nature of T_{av}, for subsets before and after 1992, broadens the peak. The combined effects are evident in Fig. 2.
9. M varies little throughout a sequence compared with T, and results based on individual M values at either the beginning or at the end of the T_i intervals are indistinguishable from those based on M_{av}.
10. R. A. Harris and P. Segall, *J. Geophys. Res.* **92**, 7945 (1987).
11. J. Langbein, unpublished data. Short baseline creepmeters do not measure the off-fault deformation present in the creep-to-locked transition zone.
12. As the sampling window approaches the end of the database, progressively more open-ended intervals are encountered and T_i is unknown because the next event in the sequence has not yet occurred.
13. J. O. Langbein, R. O. Burford, L. E. Slater, *J. Geophys. Res.* **95**, 2533 (1990).
14. R. E. Burgmann, R. E. Fielding, J. Sukhatme, *Geology* **26**, 559 (1998).
15. We found an 18% increase in M for a 10-fold increase in the preceding T_i, supporting a fault-healing process. Laboratory data suggest 3 to 8% for a 10-fold increase in recurrence interval [J. Dieterich, *J. Geophys. Res.* **77**, 3690 (1972); C. Scholz, P. Molnar, T. Johnson, *ibid.*, p. 6382; C. Scholz and T. Engelder, *Int. J. Rock Mech. Miner. Sci.* **13**, 149 (1976)].

16. Supported by the U.S. Geological Survey through award 1434-95-G2540. Data processing at the Lawrence Berkeley National Laboratory was supported by the U.S. Department of Energy Office of Basic Energy Sciences. Partial support (R.N.) came from the Lawrence Livermore National Laboratory Institute of Geophysics and Planetary Physics Campus–Laboratory Collaboration project.

19 February 1999; accepted 11 June 1999

Detection of Low-Temperature Hydrothermal Fluxes by Seawater Mg and Ca Anomalies

Stephanie de Villiers* and Bruce K. Nelson

Geochemical fluxes into and out of the ocean control its chemical composition. Measurements of the magnesium (Mg) content of seawater, an assumed "conservative" element in the ocean, reveal mid-depth Mg depletions in the vicinity of the East Pacific Rise. The magnitude of the anomalies suggests that fluxes associated with the low-temperature circulation of seawater through axial mid-ocean ridge systems are much larger than the high-temperature axial component. A higher total axial hydrothermal flux provides a mechanism that simultaneously satisfies the mass balance requirement of several major seawater constituents.

The most abundant elements enter the oceans dissolved in river water and in high-temperature (HT) hydrothermal flows at mid-ocean ridge spreading centers and are removed by calcium carbonate deposition, loss at the air-sea interface, and evaporite deposition. Given the best estimates of the global magnitude of these fluxes (*1–3*), inputs exceed outputs by perhaps a factor of 4 in the case of sodium, a factor of 2 to 10 in the case of magnesium and sulfate, and a factor of 20 for potassium. In contrast, calcium is apparently removed from the ocean at twice the rate it is supplied (*4*). Either the ocean is far removed from a steady state with respect to all major elements—accumulating Na^+, Mg^{2+}, K^+, and $SO_4{}^{2-}$, while decreasing in Ca^{2+}—or one or more significant geochemical fluxes are unrecognized or poorly constrained. Here we present evidence for the existence of the proposed large low-temperature (LT) component of hydrothermal circulation at a mid-ocean ridge axial system (*5, 6*).

Recent water column profiles show an excess of Ca over that predicted by alkalinity (*7*). It has been hypothesized that the inferred excess Ca flux originates in LT, diffuse, on-axis flows, exceeding the better documented HT discrete axial flux by a factor of up to 10 (and comparable to river input). The LT flux simultaneously resolved the Ca alkalinity discrepancy and balanced the oceanic Ca cycle (*4*). LT flux should also be an important component of other major element cycles.

It has been inferred that LT hydrothermal processes act as a sink of unknown magnitude for the other major seawater elements: Na^+, Mg^{2+}, K^+, and $SO_4{}^{2-}$ (*6, 8*), a hypothesis that is qualitatively consistent with observed deficiencies that have been noted in mass balance models of a steady-state ocean (*1–3*). Thus, the

Geological Sciences Department, Box 35-1310, University of Washington, Seattle, WA 98195-1310, USA.

*Present address: Department of Geological Sciences, University of Cape Town, Rondebosch 7701, South Africa. E-mail: steph@cigc.uct.ac.za